Research Article

Huseyin Ozan Tekin*, Ghada ALMisned*, Hesham M. H. Zakaly, Abdallah Zamil, Dalia Khoucheich, Ghaida Bilal, Lubna Al-Sammarraie, Shams A. M. Issa, Mohammed Sultan Al-Buriahi, Antoaneta Ene*

Gamma, neutron, and heavy charged ion shielding properties of Er^{3+}-doped and Sm^{3+}-doped zinc borate glasses

https://doi.org/10.1515/chem-2022-0128
received December 22, 2021; accepted January 19, 2022

Abstract: This study aimed to investigate the nuclear radiation shielding properties of erbium (Er)-reinforced and samarium (Sm)-reinforced borate glasses. In the 0.015–15 MeV photon energy range, attenuation coefficients, as well as half-value layer tenth-value layers, and the mean-free path have been calculated. Additionally, effective, and equivalent atomic numbers, effective atomic weight, electron density, and exposure and energy absorption build-up factors were also calculated. To evaluate the overall nuclear radiation attenuation competencies of Er-rich and Sm-rich glasses, effective removal cross-section values for fast neutrons and projected range/mass stopping power values for alpha and proton particles were also determined. The glass sample BZBEr2.0 had the highest linear and mass attenuation coefficients (μ and μ_m), effective conductivity (C_{eff}), the effective number of electrons (N_{eff}), and effective atomic number (Z_{eff}) values as well as the lowest half-value layer ($T_{1/2}$), tenth value layers ($T_{1/10}$), mean free path (λ), exposure build-up factor, and energy absorption build-up factor values. μ_m values were reported as 2.337, 2.556, 2.770, 2.976, 2.108, 2.266, 2.421, 2.569, and 2.714 for BZBEr0.5, BZBEr1.0, BZBEr1.5, BZBEr2.0, BZBSm0.0, BZBSm0.5, BZBSm1.0, BZBSm1.5, and BZBSm2.0 glass samples at 0.06 MeV, respectively. The results showed that Er has a greater effect than Sm regarding the gamma-ray shielding properties of borate glasses. The results of this investigation could be used in further investigations and added to older investigations with the same aim, to aid the scientific community in determining the most appropriate rare-earth additive, to provide adequate shielding properties based on the requirement.

Keywords: gamma shielding, samarium, erbium, borate glasses, glass shields

*** Corresponding author: Huseyin Ozan Tekin,** Department of Medical Diagnostic Imaging, College of Health Sciences, University of Sharjah, 27272, Sharjah, United Arab Emirates; Computer Engineering Department, Istinye University, Faculty of Engineering and Natural Sciences, Istanbul 34396, Turkey, e-mail: tekin765@gmail.com
*** Corresponding author: Ghada ALMisned,** Department of Physics, College of Science, Princess Nourah Bint Abdulrahman University, Riyadh, Saudi Arabia, e-mail: gaalmisned@pnu.edu.sa
*** Corresponding author: Antoaneta Ene,** Department of Chemistry, Physics, and Environment, Dunarea de Jos University of Galati, INPOLDE Research Center, Faculty of Sciences and Environment, 47 Domneasca Street, 800008 Galati, Romania, e-mail: aene@ugal.ro
Hesham M. H. Zakaly: Institute of Physics and Technology, Ural Federal University, Ekaterinburg 620002, Russia; Physics Department, Faculty of Science, Al-Azhar University, Assiut, 71452, Egypt
Abdallah Zamil, Dalia Khoucheich, Ghaida Bilal, Lubna Al-Sammarraie: Department of Medical Diagnostic Imaging, College of Health Sciences, University of Sharjah, 27272, Sharjah, United Arab Emirates
Shams A. M. Issa: Physics Department, Faculty of Science, Al-Azhar University, Assiut, 71452, Egypt; Department of Physics, Faculty of Science, University of Tabuk, Tabuk, Saudi Arabia
Mohammed Sultan Al-Buriahi: Department of Physics, Sakarya University, Sakarya, Turkey

1 Introduction

Gamma and X-ray are the most common types of ionizing radiation emitted and used in nuclear medicine, radiation therapy, and nuclear reactors. As these rays have no mass, they can easily travel long distances through the air [1]. As a result, gamma and X-ray are thought to be the most penetrating and difficult to shield. When a high radiation dosage is absorbed, it may result in radiation sickness, organ failure, skin rashes, carcinogenesis, genetic damage, bone-marrow loss, and death. Consequently, radiation shielding, and safety is becoming a more widespread research subject. The radiation must be reduced to safe levels by the shielding materials to protect medical

professionals, patients, and the public against the harmful impacts of ionizing radiation. Due to its cheap cost, simplicity of availability, and flexibility to be molded into any form or size, concrete is the most often used shielding material in nuclear reactors and cyclotrons. However, the use of concrete has several limitations. These include cracks in concrete that occur after extended use, the presence of water in concrete decreases the density and structural strength of the material. As concrete absorbs nuclear radiation, it heats up, causing water to evaporate, causing instability in shielding parameters calculations and inhomogeneity in the material's composition. Concrete is nonportable, making transporting it from one location to another impossible. Moreover, concrete is opaque by nature, which makes it difficult to see through [2]. Lead and lead-based compounds are also extensively used as shielding materials in hot labs and transport of radioactive materials; however, the toxic effects of lead and lead-based compounds on human health and the environment are numerous. Lead toxicity necessitates the resolution of several hygiene challenges, including dosage monitoring, supplementary protective equipment, worker training, and correct waste disposal [3]. Thus, it becomes essential to look for better shielding materials than concrete and lead. A material that incorporates transparency, nontoxicity, and radiation shielding potential is currently of great interest in the medical field. Steel, alloys, polymers, gemstones, and glasses have all been tested for their shielding properties. Glass, which has the virtue of being transparent in the visible spectrum, maybe the best possible substitute for concrete-based shielding [4–6]. Glasses are unique in their ability to accommodate a wide range of elements. As a result of this property, they can serve as a shield against harmful ionizing radiation. Zinc borate glasses and lead-free compounds with high chemical resistance, transparency, and radiation protection are being explored as possible replacements. Borate (B_2O_3) is a compound with the highest glass formation tendency because molten B_2O_3 does not crystallize by itself even when cooled at the slowest rate. Recent publications have discussed the X-ray and gamma-ray shielding capabilities of several glasses containing barium oxide (BaO), including $BaO:B_2O_3$:fly ash glass [7]. PbO, Bi_2O_3 [8–11], and BaO in borate glass [7,12], and silicate glasses [13–16], and $PbO:BaO:P_2O_5$ glass [17]. These investigations demonstrate that BaO may be used effectively in various glass matrices as a radiation shielding material. This is owing to BaO's high effective atomic number and its great X-ray and gamma-ray absorption. In a study done in 2017, ZnO was added to the glass to improve its transparency [7]. When B_2O_3 is added to glass material, it confers to the glass many valuable properties such as improving the fusibility, increasing the mechanical resistance, and high thermal resistance [18]. Osman et al. conducted research to examine the shielding parameters of glass systems from lead against neutrons and gamma rays. Attenuation parameters were evaluated and theoretically calculated using cylindrical soda-lime-silica glass samples, and lead oxide was added in various percentages to make the mixtures by weight as simple as possible. Their results indicated that the displayed spectra exhibit a similar shape and photon attenuation behavior across the investigated composites [19]. Tekin et al. conducted another significant investigation on phosphate glass materials due to their ethereality in a large spectrum range between infrared and ultraviolet, making them suitable for producing optical fibers, shielding material for radiation detection, and sensing applications. Numerous features of phosphate glass materials were discovered when the lead oxide was added to phosphate-glass samples. Lead oxide is an effective shielding material for high-energy nuclear radiations [20]. The literature review showed that different types of additives could be used for the improvement of nuclear radiation shielding properties of different glass structures. This has encouraged us to perform a comprehensive investigation on numerous glass samples in terms of their attenuation competencies against different types of radiations such as gamma, fast neutrons, and charges particles (alpha and proton). Accordingly, BZBEr [21] and BZBSm [22] glass systems were selected to study the gamma shielding properties using Phy-X/PSD [23] and Py-MLBUF [24] online platforms for energy levels between 0.015 and 15 MeV. Besides, rare earth-doped phosphate glass gives such excellent improvement in the development of many optical devices [25]. It gives higher emission efficiency with the enhancement in emission line from visible to the infrared spectral region under suitable excitation conditions as reported elsewhere [26]. Among the rare-earth ions, Er^{3+} ion has higher potential application in developing the optical and laser device. The presence of Er^{3+} ion in phosphate glass can generate 1.54 μm wavelengths, which can be utilized for optical amplification, and its visible up conversion emission can be used as a solid-state laser [27]. In this study, it was hypothesized that various types of reinforcements (e.g., Er and Sm) used to optimize the characteristics of glass will also change the basic properties of glass that protect against nuclear radiation. Therefore, it was sought to identify the potential effect of erbium (Er) and samarium (Sm) additives on the protective properties of these glasses against nuclear radiation. This study aims to search for a new, highly efficient, and environmentally friendly protective material that can replace lead or lead-based shielding materials in different types of radiation facilities. The effectiveness and quality of each sample as the additive increases will be checked and discussed. The results of this investigation

can be used in further investigations and added to previous investigations for the same purpose.

2 Materials and methods

Table 1 contains the sample codes along with the elemental compositions, densities, and weight fractions of the glass samples. The linear attenuation coefficient expresses the percent of photons that are attenuated when they travel through a certain thickness of a material. To get the linear attenuation linear attenuation coefficients value, one must examine the reactions of the material with ionizing radiation photoelectric effect, Compton scattering, and pair production (PE, CS, and PP). As shown in the following equation (1), the Beer–Lambert law is used to compute the μ value:

$$I = I_0 e^{-\mu x} = I_0 e^{-\mu_m t}, \tag{1}$$

where (I) is the intensity of gamma-ray after it has been transmitted through an absorber, and (I_0) is the initial intensity of the gamma-ray [28]. The μ represents the linear attenuation coefficient value, which is given by cm^{-1}. The mass attenuation coefficient (μ_m) is an important quality, which provides critical and basic information regarding the glass sample's ability to attenuate the intensity of the gamma radiation. Next, μ_m were calculated using equation (2).

$$\mu_m = \sum_i w_i (\mu/\rho)_i, \tag{2}$$

where w_i is the weight fraction of the ith constituent element, μ is the linear attenuation coefficient, and ρ is the density [28,29]. The half-value layer $T_{1/2}$ is basically the required thickness of the glass sample that can make the radiation intensity get reduced to one-half of its initial value. The $T_{1/2}$ is an important quality that determines whether the glass sample works sufficiently as a shielding material [30]. Similarly, to the $T_{1/2}$, we have the tenth-value layer $T_{1/10}$; which is the required thickness of the glass sample to reduce the radiation intensity to one-tenth of its initial value [31]. The way we calculate the half value layer (HVL) and the $T_{1/10}$ is by using the following equations: equations (3) and (4).

$$T_{1/2} = \frac{\mathrm{Ln}(2)}{\mu}, \tag{3}$$

$$T_{1/10} = \frac{\mathrm{Ln}(10)}{\mu}. \tag{4}$$

A mean free path λ is the mean range traveled by a photon before it interacts with the shielding material for photons traversing a substance, as stated by the American Nuclear Society-standard and shown in equation (5).

$$\lambda = \frac{1}{\mu}. \tag{5}$$

In addition to abovementioned parameters, effective atomic weight for absorption (A_{eff}) [32], effective electron density (N_{eff}) [33], effective atomic number (Z_{eff}) [33–35], equivalent atomic number (Z_{eq}) [36–40], and effective conductivity at 300 K (C_{eff}) [41–43] were determined for BZBEr0.5, BZBEr1.0, BZBEr1.5, BZBEr2.0, BZBSm0.0, BZBSm0.5, BZBSm1.0, BZBSm1.5, and BZBSm2.0 samples, respectively.

3 Results and discussion

Apart from the basic material features of produced glass materials, researchers continue to be intrigued by their radiation properties factors to gain a better understanding of their multifunctional behaviors [52–62]. Figure 1 demonstrates the

Table 1: Chemical compositions and densities for all glass samples

Sample code	mol%					wt%						ρ (g/cm^3)
	Er_2O_3	Sm_2O_3	BaO	ZnO	B_2O_3	B	O	Zn	Ba	Er	Sm	
BZBEr0.5	0.5	—	9.95	39.8	49.75	0.1278	0.3810	0.3091	0.1623	0.0199	—	3.42
BZBEr1.0	1.0	—	9.90	39.6	49.50	0.1249	0.3753	0.3022	0.1586	0.0390	—	3.451
BZBEr1.5	1.5	—	9.85	39.4	49.25	0.1221	0.3697	0.2955	0.1551	0.0575	—	3.492
BZBEr2.0	2.0	—	9.80	39.2	49.00	0.1195	0.3644	0.2890	0.1517	0.0754	—	3.512
BZBSm00	—	0.0	10.0	40.0	50.00	0.1307	0.3869	0.3163	0.1661	—	—	3.36
BZBSm0.5	—	0.5	9.95	39.8	49.75	0.1280	0.3818	0.3097	0.1626	—	0.0179	3.412
BZBSm1.0	—	1.0	9.90	39.6	49.50	0.1254	0.3767	0.3034	0.1593	—	0.0352	3.442
BZBSm1.5	—	1.5	9.85	39.4	49.25	0.1228	0.3719	0.2972	0.1560	—	0.0520	3.474
BZBSm2.0	—	2.0	9.80	39.2	49.00	0.1204	0.3672	0.2912	0.1529	—	0.0683	3.493

changes of μ with energy. It is evident from the graph that there is a sharp decrement from 0.015 to 0.030 MeV, which demonstrates the dominance of photoelectric absorption. Then, a sudden change occurred in the energy range from 0.03 to 0.04 MeV, which is a result of the K-absorption edge of the two elements (Er = 0.0574 MeV and Sm = 0.0468 MeV) [44]. Following that, a sudden decrement in the μ values was seen again in the energy range of (0.05 MeV to around 1 MeV). After 1.02 MeV, a smooth decrement is a result of PP, which usually happens in the high-energy range. The increment of Er and Sm in the glasses increases the values of the μ. For example, μ values for BZBEr1.0, BZBEr1.5, and BZBEr2.0 at 0.015 MeV was reported as 136.860, 142.930, and 148.030, respectively. In addition, as the energy increases, the μ values decrease. According to this study, it is observed that BZBEr2.0 has the highest μ value. The mass attenuation coefficient expresses the chance of incoming photons interacting with unit mass/unit area stuff. As observed in the

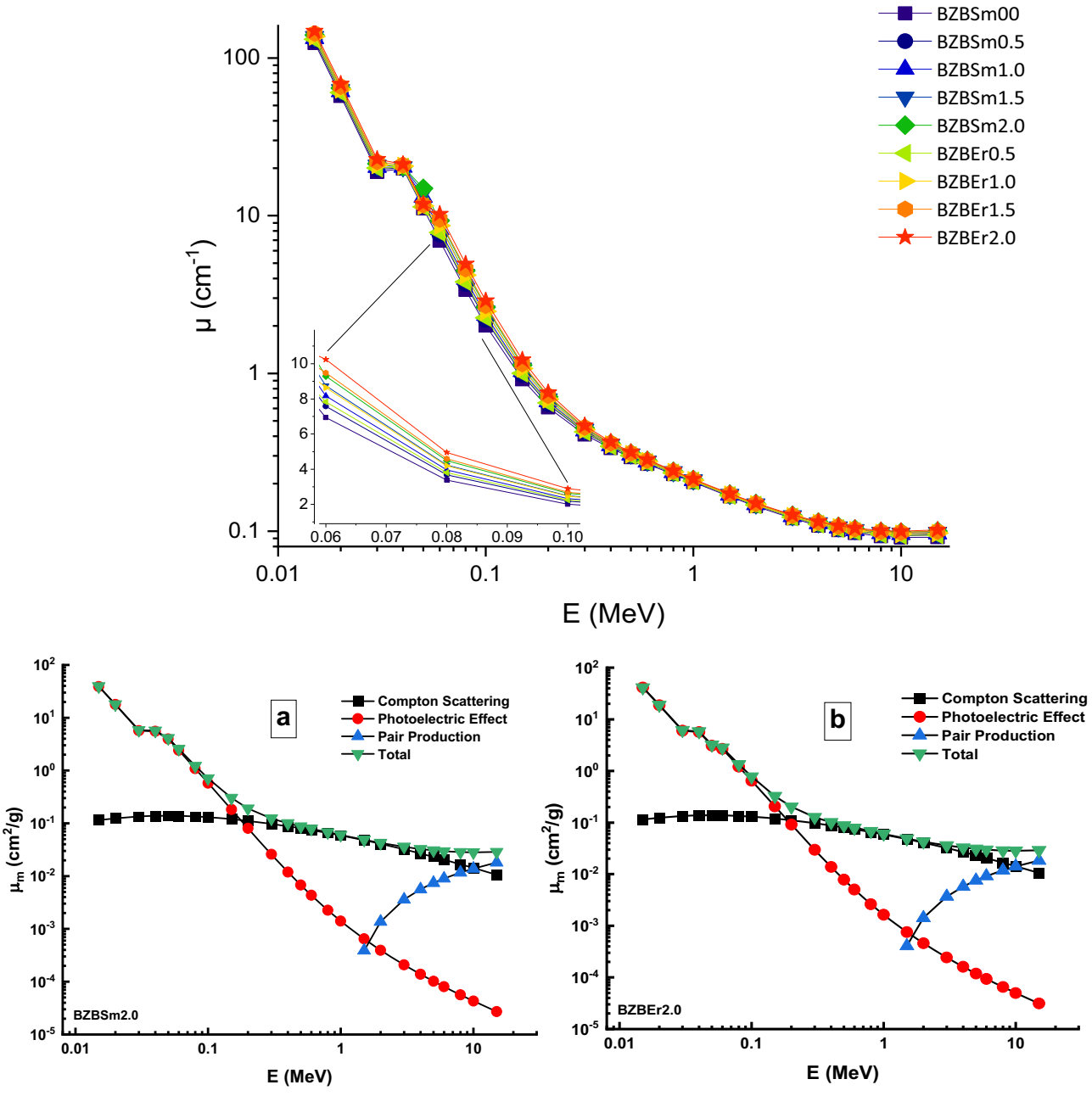

Figure 1: Variation of linear attenuation coefficient (μ) against photon energy for BZBEr and BZBSm glasses while the contribution of PE, CS, and PP with (a) BZB SM2.0 sample and (b) BZBEr2.0 sample.

graph in Figure 2, when the energy increases, the total μ_m decreases. The tendency of μ_m is like μ; therefore, similar behaviors were obtained for both parameters. Figure 2 shows variation of mass attenuation coefficient (μ_m) against photon energy for (a) BZBEr and (b) BZBSm glasses. The maximum value of μ_m is reported at 0.015 MeV. As the energy increased, a sharp decrement was reported in the energy range from 0.015 MeV to around 0.03 MeV. This is due to the PE predominance at low energies. Furthermore, a sudden change occurred in the energy range (0.030–0.0.040 MeV) because of the K-absorption edge effect. Moreover, it has been reported that as the percentage of the additives (Er and Sm) increases in the glass sample, the mass attenuation coefficient increases as well. According to this study, it has been reported that BZBEr2.0 has the greatest μ_m value and BZBSm0.0 has the lowest μ_m value. For example, at 0.06 MeV, the obtained values for BZBEr0.5, BZBEr1.0, BZBEr1.5, BZBEr2.0, BZBSm0.0, BZBSm0.5, BZBSm1.0, BZBSm1.5, and BZBSm2.0 are, respectively, as follows: 2.337, 2.556, 2.770, 2.976, 2.108, 2.266, 2.421, 2.569, and 2.714 cm^2/g. The half-value layer ($T_{1/2}$) is a very important shielding parameter that was also investigated in this study. A lower $T_{1/2}$ value indicates a more efficient and useful shielding material. Figure 3 shows the variations in the $T_{1/2}$ as the incident photon energy of the glass samples changes starting from 0.015 all the way upto 15 MeV. As demonstrated, the $T_{1/2}$ of all the glass samples increases at a similar rate as the energy increases, meaning they have a positive correlation. At the photon energy equal to 0.015 MeV, the samples BZBEr0.5, BZBEr1.0, BZBEr1.5, BZBEr2.0, BZBSm0.5, BZBSm1.0, BZBSm1.5, and BZBSm2.0 all started with a $T_{1/2}$ equal to 0.005 cm, whereas the remaining sample BZBSm0.0 started from a $T_{1/2}$ equal to 0.006 cm. The samples have very similar $T_{1/2}$ values and grow in a similar manner. At the maximum photon energy 15 MeV, the sample BZBEr2.0 had the lowest $T_{1/2,}$ equal 6.8164 cm. However, this value is not that big of a difference compared to the other samples, such as BZBEr1.5 and BZBSm2.0, which both had $T_{1/2}$ approximately equal to 6.9 cm. As shown Figure 4, the half value layer $T_{1/2}$ values of the investigated BZBEr2.0 and BZBSm2.0 samples dependent on photon energy at specific energies and compared with Glass1 [45], Glass2 [46], Glass3 [47], Glass4 [48], Glass5 [49], Glass6 [8], Glass7 [50], Glass8 [51], and standard shielding materials (ordinary concrete: OC [52], and hematite–serpentine concrete: HSC [28]), where BZBEr2.0 and BZBSm2.0 samples are lower than the $T_{1/2}$ values of all samples even OC and HSC. The tenth-value layer $T_{1/10}$ is quite close to the HVL definition in terms of significance as it is the thickness of the shielding glass material necessary to lower the initial intensity to a tenth (10%) of its value. A single $T_{1/2}$ is equal to 0.3 $T_{1/10}$. In Figure 5, the relation between the $T_{1/10}$ of the glass samples and the incident photon energy is comprehensively demonstrated for all investigated glass samples. Glass samples had their lowest $T_{1/10}$ values at the lowest photon energy (0.015 MeV); the TVL for the samples BZBEr1.5 and BZBEr2.0 was both equal to 0.016 cm. The samples BZBEr1.0, BZBSm1.0, BZBSm1.5, and BZBSm2.0 had a $T_{1/10}$ equal to 0.017 cm, whereas the samples BZBEr0.5 and BZBSm0.5 had a $T_{1/10}$ of 0.018 cm. Consequently, the remaining sample BZBSm0.0 had the highest $T_{1/10}$ equal to 0.019 cm. The samples continue to overlap and increase all the way until the maximum photon energy (15 MeV), where a single sample seems to have the lowest $T_{1/10}$ 22.644 cm, which is BZBEr2.0, and the

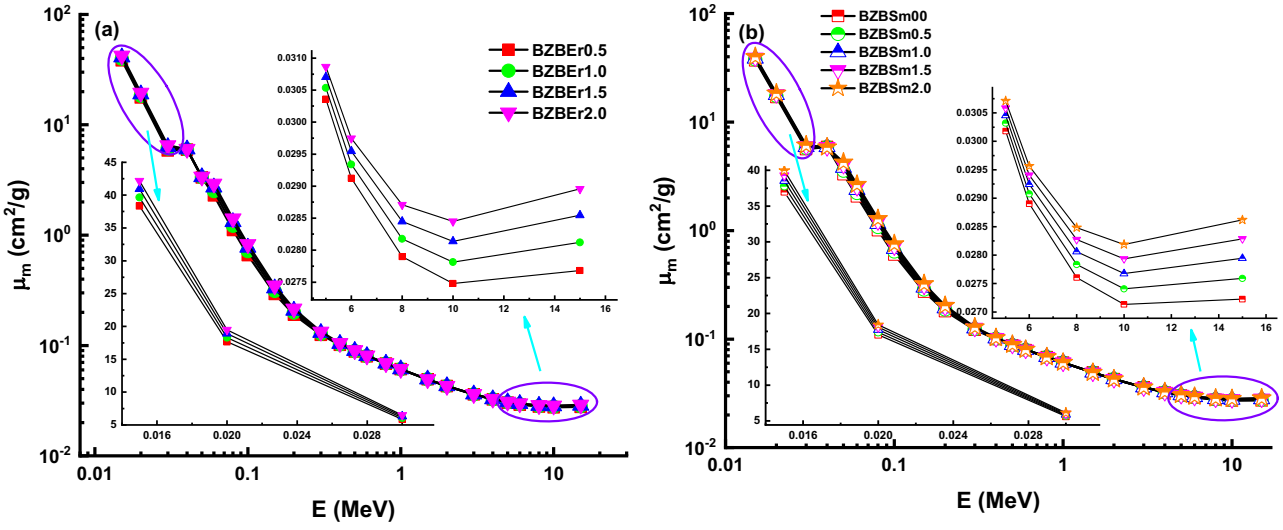

Figure 2: Variation of mass attenuation coefficient (μ_m) against photon energy for (a) BZBEr and (b) BZBSm glasses.

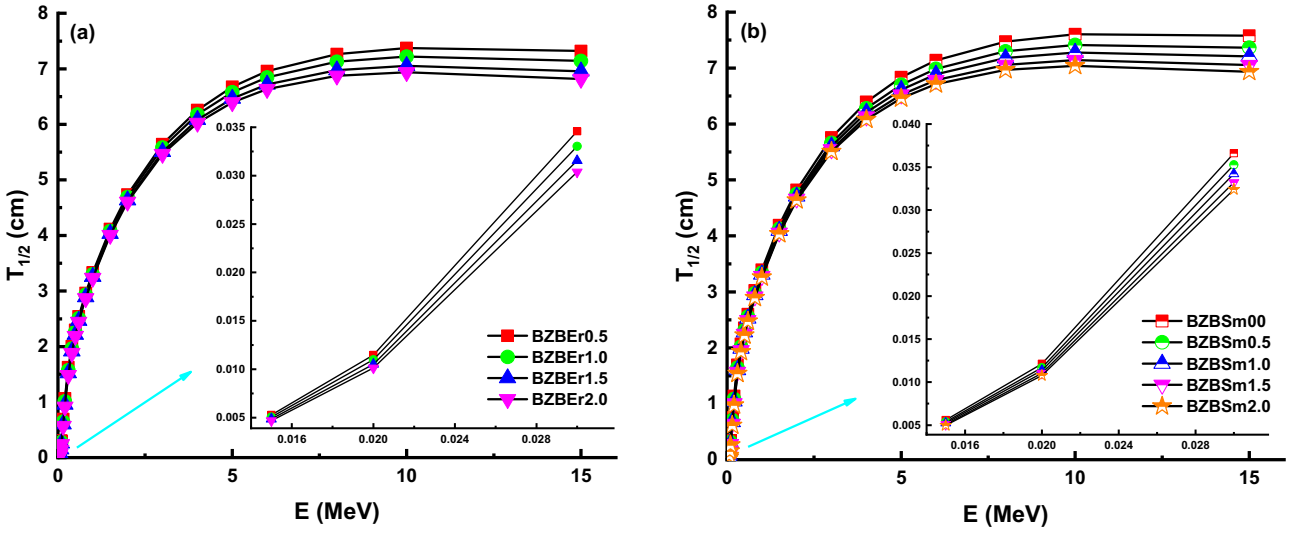

Figure 3: Variation of half value layer ($T_{1/2}$) against photon energy for (a) BZBEr and (b) BZBSm glasses.

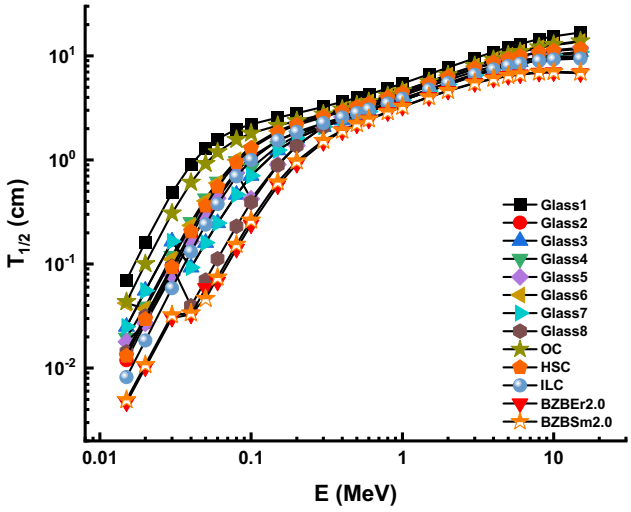

Figure 4: Half Value layer $T_{1/2}$ of the investigated glasses compared with some standard shielding materials (OC, HSC, and eight different glass samples).

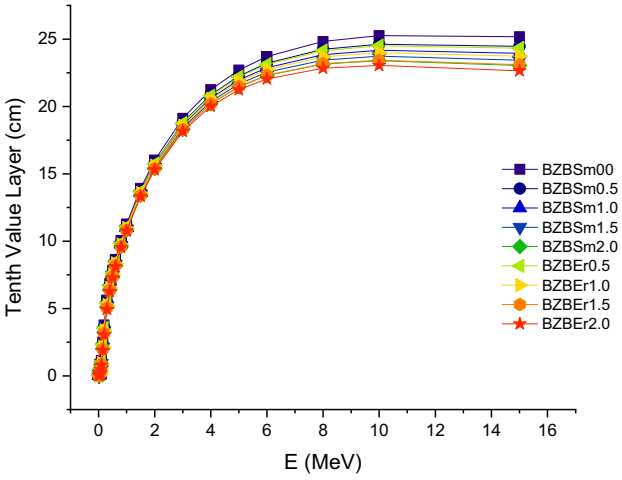

Figure 5: Comprehensive demonstration of tenth value layer values against photon energy for BZBEr and BZBSm glasses.

sample with the highest $T_{1/10}$ 25.170 cm was BZBSm0.0. However, the term of a mean free path (mfp – λ) is an essential parameter that demonstrates the average distance traveled by a photon within the glass sample before any interaction between the photon and the glass shielding material occurs. As the mfp equals $1/\mu$, it will have an inverse relation to μ, and accordingly, the mfp and μ will have opposite relations with incident photon energy. Figure 6 demonstrates the changes of the λ values compared to the incident photon energy of the glass shielding samples ranging from 0.015 to 15 MeV. Like the $T_{1/2}$ and the $T_{1/10}$, the λ increases for all samples as the photon energy increases. The λ of all the glass samples is very close in value and increases in a similar rate and manner. At the photon energy 0.015 MeV, the samples average a λ equal to 0.007 cm. Moreover, at the maximum energy of 15 MeV, they average a mfp equal to 10.318 cm, with the sample BZBEr2.0 having the lowest mfp value, which is equal to 9.834 cm. Noting that the lowest the mfp value, the better the shielding material is. The effective conductivity is a parameter that is affected by the changes in photon energies. In other words, the C_{eff} values change when the energy is changed. The maximum value of C_{eff} in Figure 7 has been reported at 0.06 MeV, which is 26.108 S/m for BZBEr2.0. Starting from 0.015 MeV, a slight decrement in the C_{eff} values for all the studied elements was reported. After that, a sudden

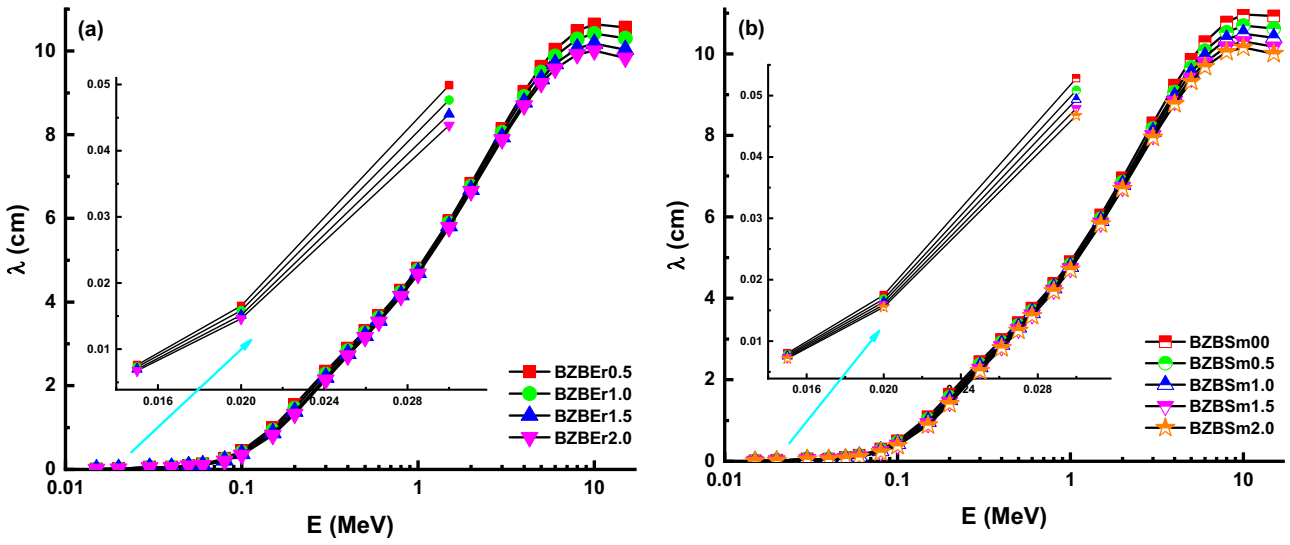

Figure 6: Variation of men free path (λ) against photon energy for (a) BZBEr and (b) BZBSm glasses.

increment is observed at 0.040 MeV because of K-absorption edge of Er and Sm. Moreover, a fluctuation has been reported from 0.040 to 0.060 MeV. According to Figure 7 BZBSm0.0 started decreasing before other elements. Additionally, it has been reported that the minimum value of C_{eff} is 6.863 S/m for BZBSm0.0 at 1.333 MeV. At the energy of 0.060 MeV, all the C_{eff} values of the elements started to decrease rapidly until the energy reached 0.4 MeV, where C_{eff} started decreasing at a very low rate. This decrement kept going on as the energy increased until it reached 1.5 MeV, where the C_{eff} values started to increase for all the elements. This increment is due to the PP, which occurs with photons of high energy. Figure 8 shows the variation of an effective number of electrons per gram N_{eff} with energy values. As seen in the graphs, N_{eff} values decreased at the beginning in the energy range, 0.015 to 0.05 MeV, where photoelectric interaction is predominant, and then a sudden increase is observed due to the K-absorption edge of the additives. Subsequently, a rapid decrease in the N_{eff} values was seen between 0.05 to 0.5 MeV, and this is where CS is prevalent. A slight increase starts from 3 MeV, where PP is dominant. The result showed that sample BZBSm1.5 has the smallest N_{eff} value, and BZBEr2.0 has the highest value. As an example, N_{eff} values were reported 3.322, 3.380, 3.434, 3.486, 3.261, 3.299, 3.334, 3.368, and 3.4 S/m, for BZBEr0.5, BZBEr1.0, BZBEr1.5, BZBEr2.0, BZBsm0.0, BZBsm0.5, BZBsm1.0,

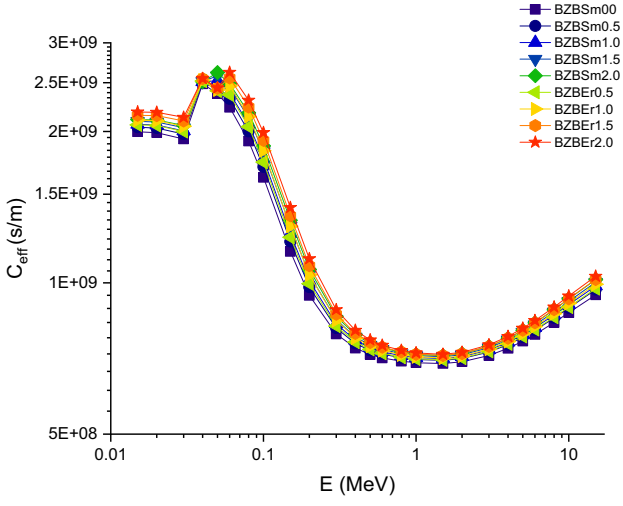

Figure 7: Variation of effective conductivity (C_{eff}) with energy (0.015–15 MeV).

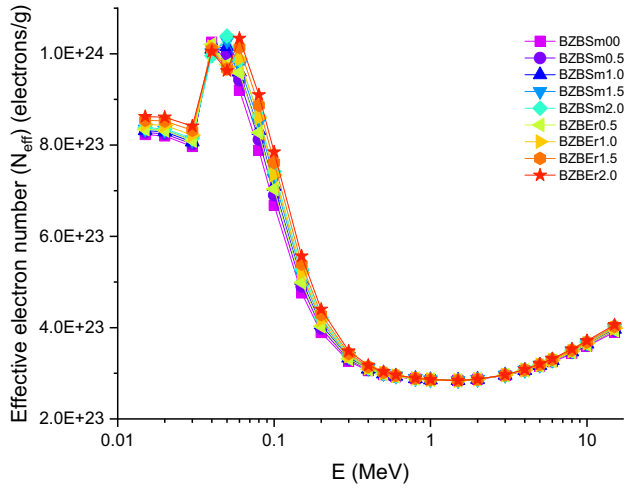

Figure 8: Variation of effective number of electrons per gram (N_{eff}) with energy (0.015–15 MeV).

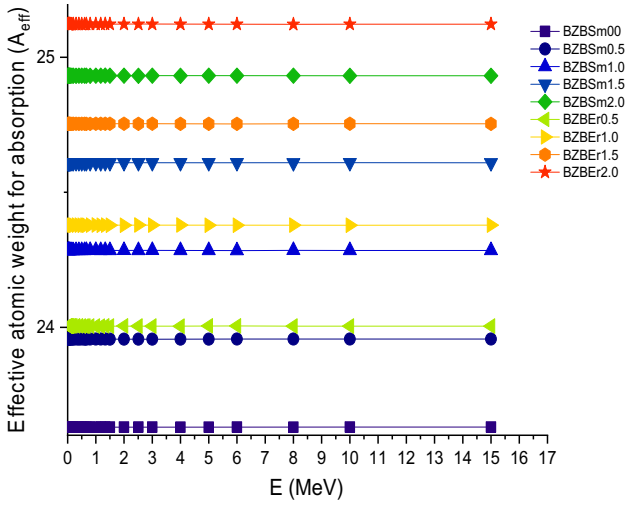

Figure 9: Variation of effective weight (A_{eff}) with energy (0.015–15 MeV).

BZBsm1.5, and BZBsm2.0 samples at 0.3 MeV. Figure 9 shows the variation in effective atomic weight absorption A_{eff} for all glasses as a function of the photon energy. The additive properties have a clear relationship with the variations in the total atomic weight of the mixture, resulting in densities ranging from 3.42 to 3.493 g/cm^3. As a result, BZBEr2.0 was found to have the highest A_{eff} value of all the glasses examined, with a value of 25.123, and BZBSm0.0 had the lowest value, 23.630. Figure 10 presents values of Z_{eff} as a function of photon energy. The term Z_{eff} is used to describe how various elemental structures react to ionizing radiation. When it comes to gamma-ray attenuation, elements with higher atomic numbers are generally thought to be superior. However, in this study, both the additives have very similar atomic numbers (Er-68 and Sm-62). Additionally, Z_{eff} is proportional to photon energy, and the discrepancy between Z_{eff} and energy may be accounted for by the photoelectric absorption, CS, and PP processes. An obvious pattern can be seen from the graph that as energy increases, Z_{eff} values decrease. The mechanisms by which photons interact with matter can provide an explanation for this fluctuation. Radiation physics notions imply that the PE dominates at low energies. As the energy level rises, the likelihood of this mechanism occurring decreases, and CS takes over as the dominant process. As PP surpasses the previous two energy >1.02 MeV processes, we can see an increase in Z_{eff} as the photon energy approaches 15 MeV. For instance, for BZBEr0.5 glass sample at 1 MeV, the Z_{eff} value was reported as 11.396, whereas at 2 MeV, Z_{eff} value was 11.443. Although, an exception for this pattern is seen at 0.04 MeV, which occurs because of the K-absorption edge values of Er and Sm. Nevertheless, there was no remarkable difference in Z_{eff} values between the glass samples at all photon energies. This may be due to minor weight and density differences between the Er and Sm substitutes. The maximum difference in Z_{eff} values is seen at 0.080 MeV as 32.983, 34.806, 36.464, 37.967, 30.964, 32.298, 33.545, 34.693, and 35.757 for BZBEr0.5, BZBEr1.0, BZBEr1.5, BZBEr2.0, BZBSm0.0, BZBSm0.5, BZBSm1.0, BZBSm1.5, and BZBSm2.0 for the glass samples in the region where the PE is dominant. From outcomes, it has been observed that Z_{eff} values of the BZBEr-encoded glass samples increased as the percentage of Er increased, and in the second glass sample (i.e., BZBSm), Z_{eff} values also increased by increasing the Sm content. The highest Z_{eff} value was reported for BZBEr2.0 glass sample with a maximum value of 43.224 at 0.6 MeV. The terms of energy

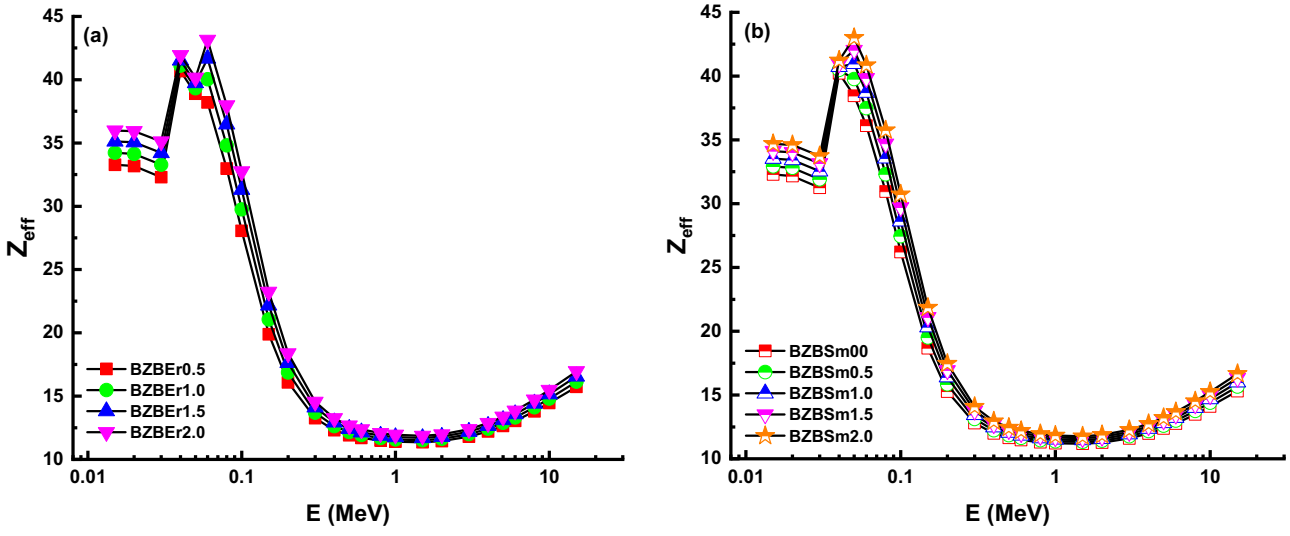

Figure 10: Variation of effective atomic number (Z_{eff}) against photon energy for (a) BZBEr and (b) BZBSm glasses.

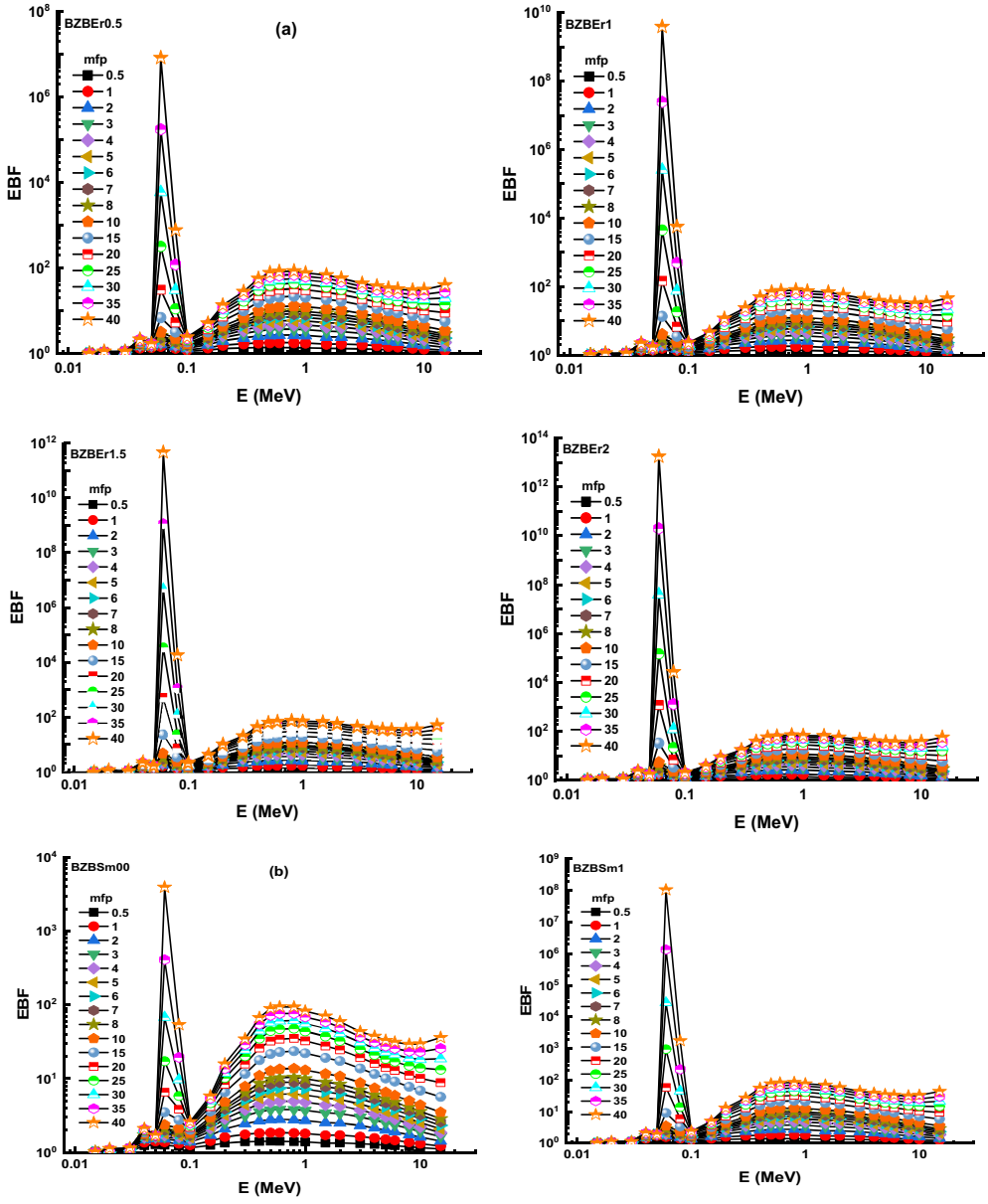

Figure 11: Variation of exposure buildup factor (EBF) against photon energy for (a) BZBEr and (b) BZBSm glasses.

absorption build-up factor (EABF) and the exposure build-up factor (EBF) are critical photon shielding characteristics that have been used to characterize scattering in irradiated materials. Figures 11 and 12 illustrate the variance in EBF and EABF values for all glass samples calculated using the geometric progression fitting approach for the energy range of 0.015–15 MeV and penetration-depths ranging from 0.5 to 40 mfp. As the precision of the shielding parameters increases, the accuracy of the radiation measurements increases as well, resulting in a reduction in the findings' abnormalities. As per the graphs in Figure 11, the EBF of the glass samples is low at low energies, increases to a maximum at medium energies, and then lowers again at high energies, where pair formation interactions occur. CS occurs when entering photons scatter with varying energies despite the photons being totally absorbed by pair formation and photoelectric absorption processes. Because this scattering facilitates the accumulation of low-energy photons in the generated glasses, the EBF values of the glasses are highest at medium energies. The sharp peaks observed in the figures are due to the K-absorption edges of the elements present in the glass samples. Additionally, the EBF curves for BZBEr and BZBSm glasses are almost identical. Almost all glass samples had

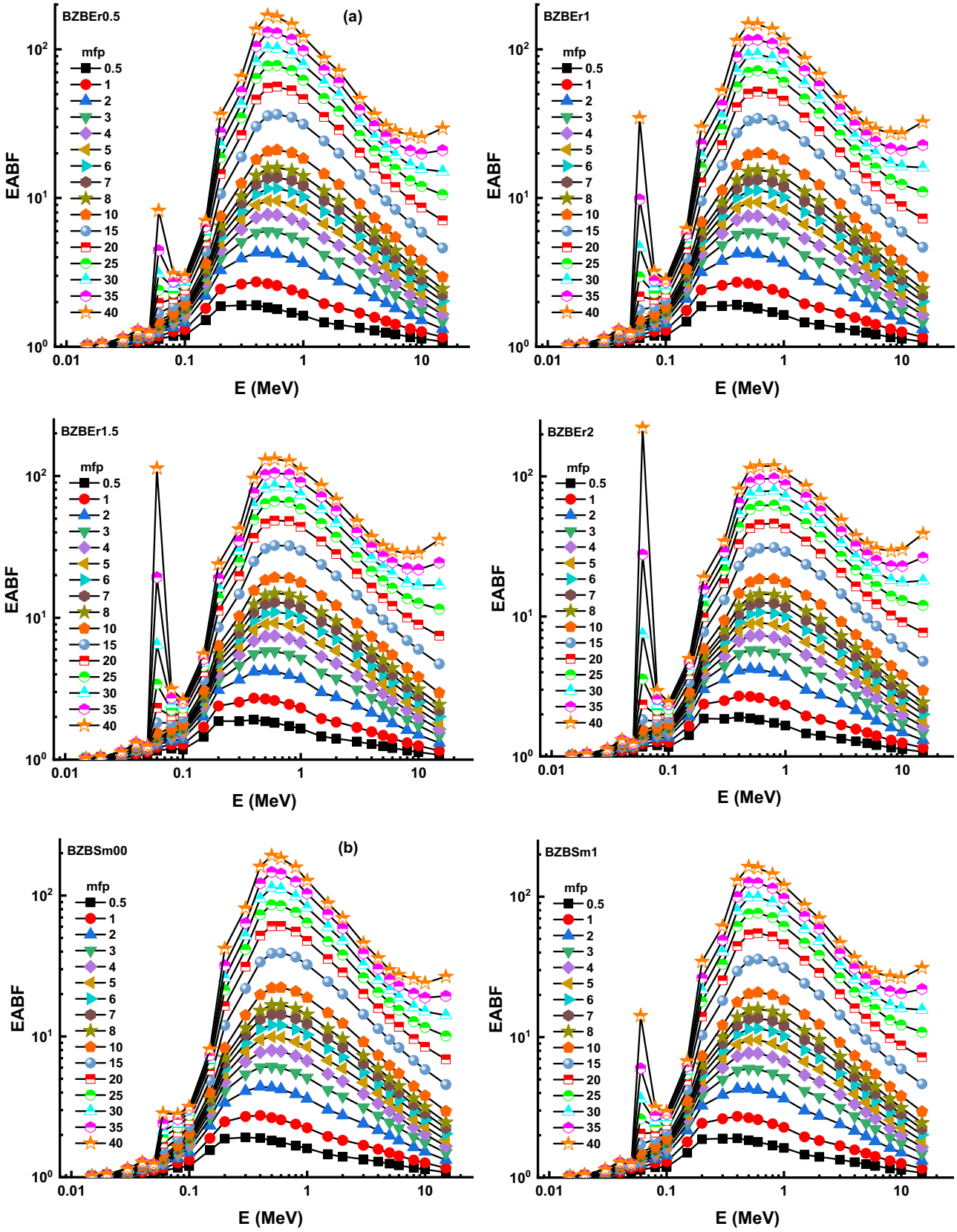

Figure 12: Variation of EABF against photon energy for (a) BZBEr and (b) BZBSm glasses.

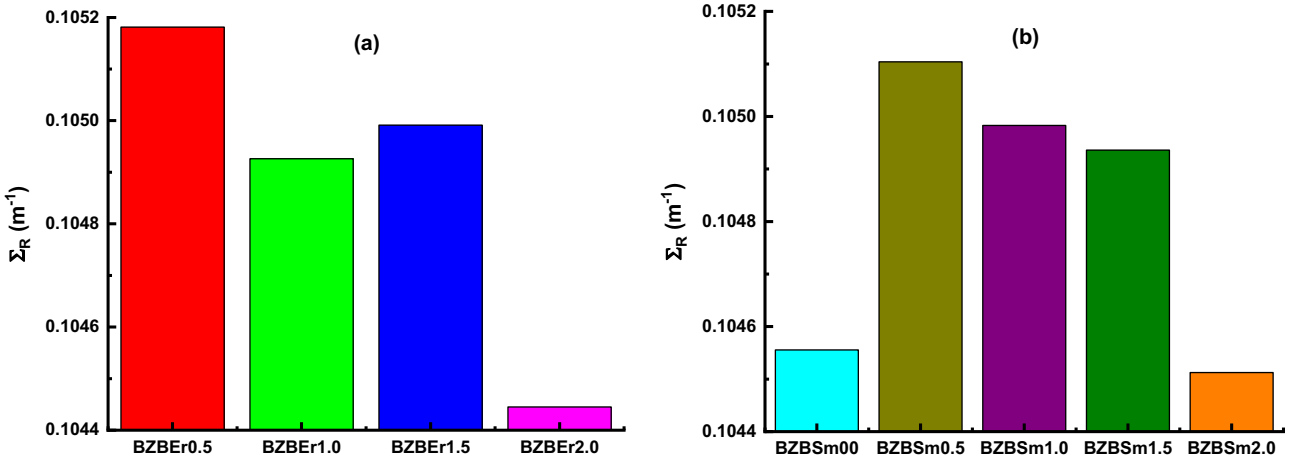

Figure 13: Effective removal cross-sections for fast neutrons (Σ_R) for (a) BZBEr and (b) BZBSm glasses.

a maximum EBF value of 0.6 MeV. EBF values are approximately the same at the lowest energies, up to 5 mfp. For example, at 2 mfp and 0.015 MeV, the EBF values of BZBEr0.5, BZBEr1.0, BZBEr1.5, and BZBEr2.0 glass samples are 1.0044, 1.0046, 1.0059, and 1.0071, respectively. As the content of Er and Sm increases, the calculated EBF values decreased. As an example, the highest EBF value decreased from 6.7321 to 6.2982 for the BZBEr glass sample, at 0.8 MeV and 6 mfp. With increasing energy, the EBF gradually increases until it reaches its maximum at a high penetration depth. For instance, for BZBSm0.0-coded glass sample, at 0.5 MeV, the EBF value at 0.5 mfp was 1.404, and at 10mfp the value was 12.004. This makes it apparent that as the mfp increases, EBF values increase as well. According to the study, BZBSm0.0 has the highest EBF value and BZBEr2.0 has the lowest value. This is an excellent demonstration of how effectively materials can guard against gamma radiation. As a result, BZBEr2.0 with the lowest EBF values may be considered the appropriate sample among the glass samples studied. As for EABF, it is a quantity influenced by the amount of energy in the substance as well as the detector function in the interacting material. A trend like that seen in EBF graphs is observed. Hence, it can be noted from Figure 12 that BZBSm0.0 has the highest EABF value, and BZBEr2.0 has the lowest value. The current investigation additionally examined the produced glass specimens' fast neutron shielding capability. When a fast neutron engages with an absorbing medium,

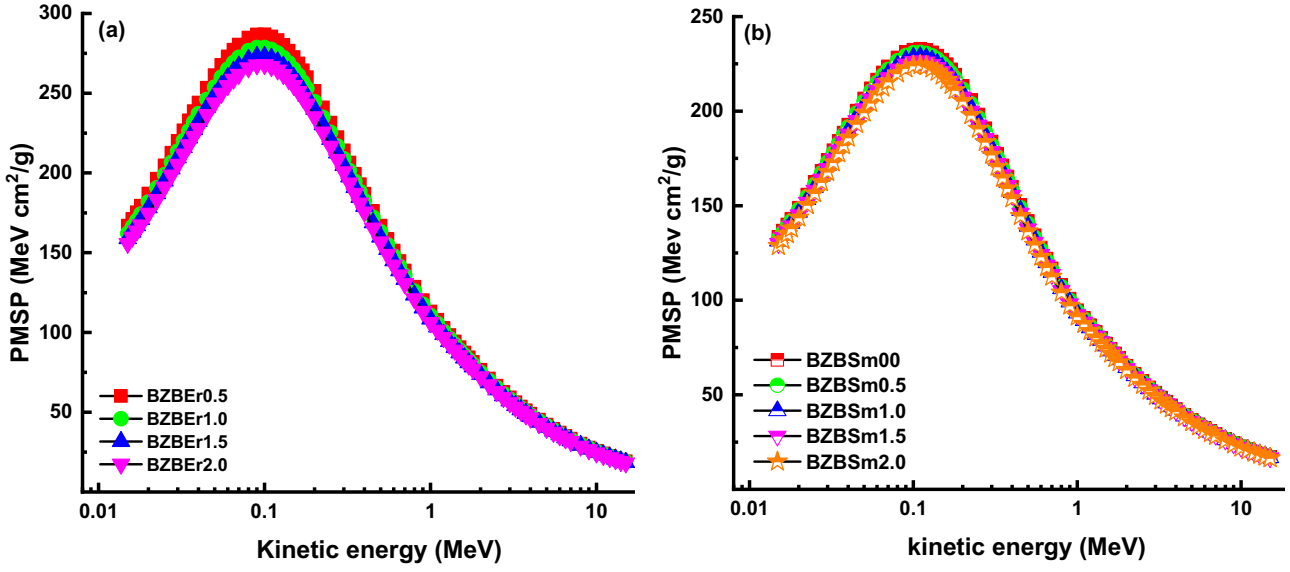

Figure 14: PMSP as a function of kinetic energy for (a) BZBEr and (b) BZBSm glasses.

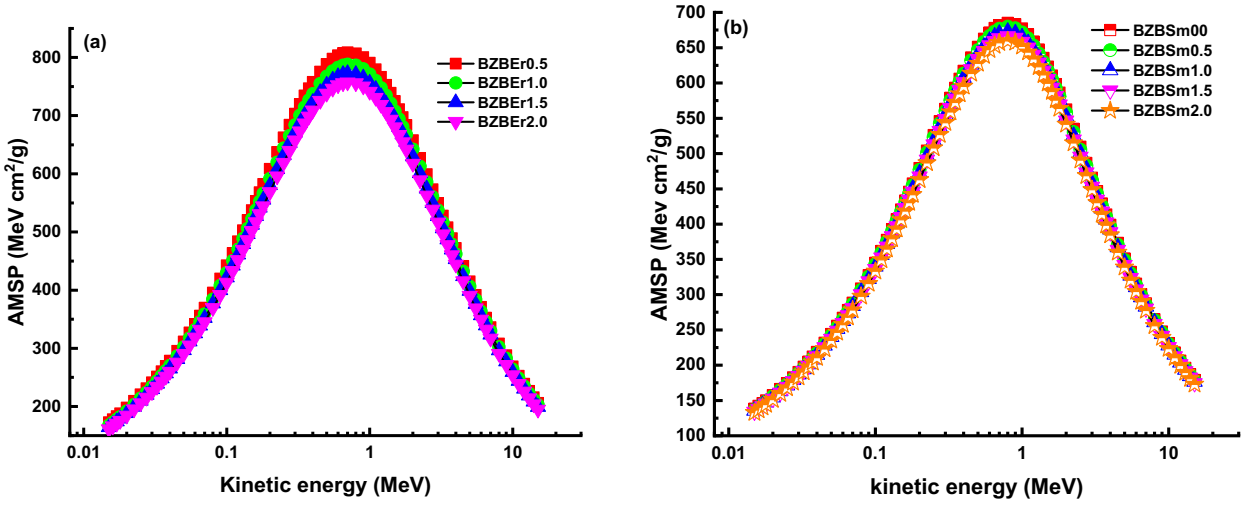

Figure 15: AMSP as a function of kinetic energy for (a) BZBEr and (b) BZBSm glasses.

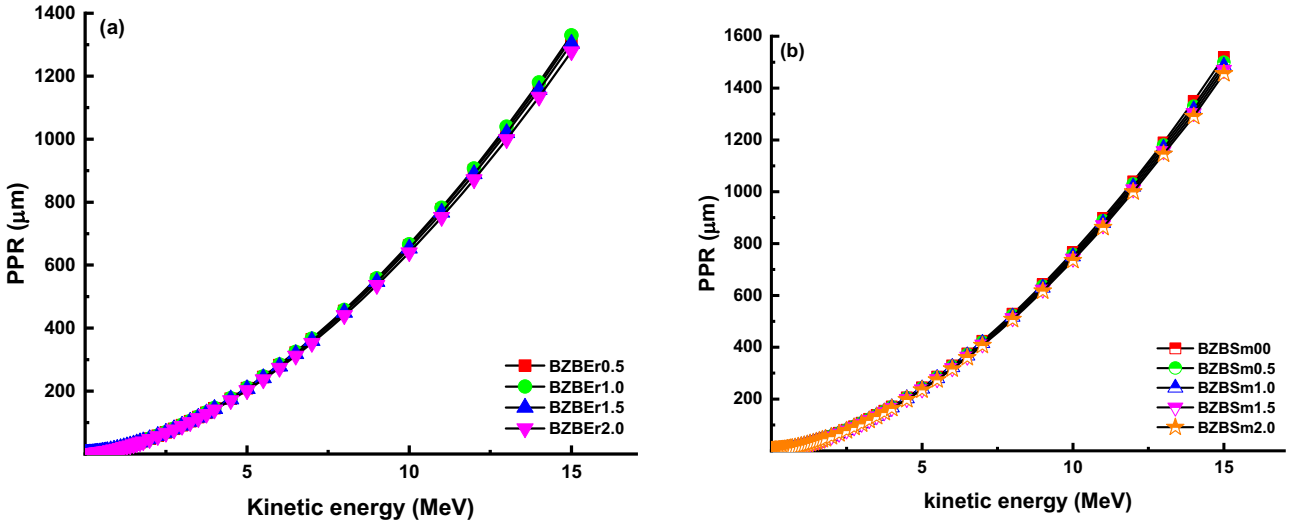

Figure 16: PPR as a function of kinetic energy for (a) BZBEr and (b) BZBSm glasses.

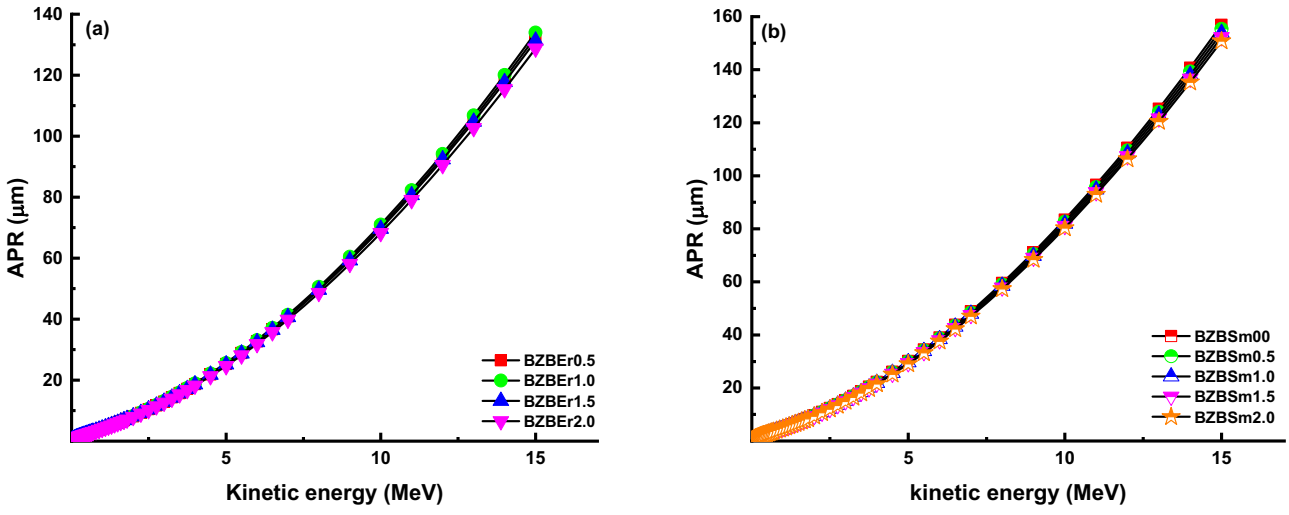

Figure 17: APR as a function of kinetic energy for (a) BZBEr and (b) BZBSm glasses.

it can take one of three distinct pathways, depending on the attenuator's composition and energy of the incident neutrons. This probability may be quantified or subjectively represented in terms of the macroscopic (or effective) cross section, or alternatively as the effective removal cross sections for fast neutrons Σ_R. The Σ_R values for the studied glass specimens are shown in Figure 13. The Σ_R values were reported as 0.1051, 0.1049, 0.1049, 0.1044, 0.1045, 0.1051, 0.1049, 0.1049, and 0.1045 cm^{-1} for BZBEr0.5, BZBEr1.0, BZBEr1.5, BZBEr2.0, BZBSm0.0, BZBSm0.5, BZBSm1.0, BZBSm1.5, and BZBSm2.0, respectively. As it can be observed from the reported numerical values, there are differences between the Σ_R values of the studied glass samples. However, among the investigated glass specimens, the BZBSm0.5 glass exhibits the highest fast neutron shielding capability. Finally, we will briefly address the ability of the investigated glass specimens to protect against charged particles (e.g., proton and alpha particles). According to Coulomb's law, a charged particle interacts with a substance. As a result, these particles may collide several times before losing all their kinetic energy. Stopping power (SP) and particle ranges may be used to quantify the charged particle's gradual loss of energy through matter (PR). Figures 14–17 display the effect of increasing kinetic energy on the proton mass stopping power (PMSP), alpha mass stopping power (AMSP), proton projected range (PPR), and alpha projected range (APR) values of the examined glasses obtained from SRIM code [63]. The given comprehensive graphs depict that the attenuation properties of the studied glasses against charged alpha and proton particles are similar. Similar elemental compositions or slight increments can explain this in Er and Sm reinforcements through glass structures. Our findings, however, indicate that the BZBEr2.0 sample with the highest Er additive has higher attenuation characteristics against alpha and proton particles. These findings may help explain the attenuation capabilities of examined glasses against charged alpha and proton particles, which are more likely to be seen than other analyzed radiation types such as gamma and fast neutrons.

4 Conclusion

Recent investigations have illustrated that lead and lead-based materials have a number of important drawbacks, including short life span, toxicity, high cost, and lack of transparency. Considering these properties, several studies have been done to examine the gamma shielding properties of rare-earth-doped glass materials because of their numerous advantages. In this study, nine different zinc borate glasses doped with Er and Sm were examined for several different nuclear shielding properties, including linear and mass attenuation coefficients, half and tenth value layers, mean free path, build up factors, and so forth. The results of this study can be summarized as follows:

i) μ_m values of 2.337, 2.556, 2.770, 2.976, 2.108, 2.266, 2.421, 2.569, and 2.714 were recorded for BZBEr0.5, BZBEr1.0, BZBEr1.5, BZBEr2.0, BZBSm0.0, BZBSm0.5, BZBSm1.0, BZBSm1.5, and BZBSm2.0 glass samples at 0.06 MeV, respectively. It is noted that BZBEr2.0 has the highest value.
ii) The findings indicated that BZBEr2.0 had the lowest $T_{1/2}$, $T_{1/10}$, and λ values at the photon energies investigated.
iii) BZBEr2.0 glass sample reported the highest Z_{eff} value.
iv) BZBEr2.0 glass sample had the highest N_{eff} and A_{eff} values
v) EBF and EABF values were the lowest for the BZBEr2.0 glass sample.

As the BZBEr2.0 with the greatest Er additive demonstrated better nuclear radiation attenuation capabilities, it was obvious that Er reinforcement had a significant favorable effect on nuclear radiation attenuation qualities. Our results indicate that Er reinforced glasses zinc glasses may be an appropriate candidate material for nuclear shielding applications. Furthermore, the findings indicate that Er is more effective at shielding nuclear radiation than Sm. According to the literature study, researchers are exploring a variety of different types of studies into additives for nuclear radiation shielding improvements. Consequently, our results may contribute to the existing body of knowledge and will aid in identifying special additives and associated glass compositions that offer the most appropriate shielding characteristics for the needs and applications.

Funding information: This study was performed under Princess Nourah bint Abdulrahman University Researchers Supporting Project Number (PNURSP2022R149), Princess Nourah bint Abdulrahman University, Riyadh, Saudi Arabia. Authors express their sincere gratitude to Princess Nourah bint Abdulrahman University.

Author contributions: H.O.T. – conceptualization, writing–original draft, supervision, writing – review and editing; G.A. – visualization, software; H.M.H.Z. – formal analysis, data curation; A.Z. – data curation, formal analysis, writing – original draft; D.K. – data curation, formal analysis, writing – original draft; G.B. – data curation, formal

analysis, writing – original draft; L.A. – data curation, formal analysis, writing – original draft, S.A.M.I. – visualization, software; and M.S.A. – visualization, software, A.E – methodology, funding acquisition through APC by "Dunarea de Jos" University 355 of Galati, Romania , resources.

Conflict of interest: There is no conflict of interest.

Ethical approval: The conducted research is not related to either human or animal use.

Data availability statement: Data available on reasonable request from the authors.

References

[1] Issa SA, Ali AM, Tekin HO, Saddeek YB, Al-Hajry A, Algarni H, et al. Enhancement of nuclear radiation shielding and mechanical properties of $YBiBO_3$ glasses using La_2O_3. Nucl Eng Technol. 2020;52(6):1297–303.

[2] Han S, Hong S, Nam S, Kim WS, Um W. Decontamination of concrete waste from nuclear power plant decommissioning in South Korea. Ann Nucl Energy. 2020;149:107795. doi: 10.1016/j.anucene.2020.107795.

[3] Mann KS, Heer MS, Rani A. Effect of low-Z absorber's thickness on gamma-ray shielding parameters. Nucl Instrum Methods Phys Res Sect A Accel Spectrometers Nucl Instrum Methods Phys Res A. 2015;797:19–28.

[4] Kurudirek M. Heavy metal borate glasses: potential use for radiation shielding. J Alloy Compd. 2017;727:1227–36.

[5] Zakaly HM, Abouhaswa AS, Issa SA, Mostafa MY, Pyshkina M, El-Mallawany R. Optical and nuclear radiation shielding properties of zinc borate glasses doped with lanthanum oxide. J Non-Cryst Solids. 2020;543:120151.

[6] Zakaly HM, Ashry A, El-Taher A, Abbady AG, Allam EA, El-Sharkawy RM, et al. Role of novel ternary nanocomposites polypropylene in nuclear radiation attenuation properties: in-depth simulation study. Radiat Phys Chem. 2021;188:109667.

[7] Chanthima N, Kaewkhao J, Limkitjaroenporn P, Tuscharoen S, Kothan S, Tungjai M, et al. Development of $BaO–ZnO–B_2O_3$ glasses as a radiation shielding material. Radiat Phys Chem. 2017;137:72–7.

[8] Al-Harbi FF, Prabhu NS, Sayyed MI, Almuqrin AH, Kumar A, Kamath SD. Evaluation of structural and gamma ray shielding competence of $Li_2O–K_2O–B_2O_3$–HMO (HMO = $SrO/TeO_2/PbO/Bi_2O_3$) glass system. Opt (Stuttg). 2021;248:168074.

[9] Perişanoğlu U, Tekin HO, Abouhaswa AS, Kavaz E. Structural and nuclear shielding qualities of B_2O_3–PbO–Li_2O glass system with different Ag_2O substitution ratios. Radiat Phys Chem. 2021;179:109262.

[10] Aboud H, Aldhuaibata MJ, Alajermi Y. Gamma radiation shielding traits of $B_2O_3–Bi_2O_3–CdO–BaO–PbO$ glasses. Radiat Phys Chem. 2021;191:109836.

[11] El Batal HA, El Batal FH, Azooz MA, Marzouk MA, El Kheshen AA, Ghoneim NA, et al. Comparative shielding behavior of binary $PbO–B_2O_3$ and $Bi_2O_3–B_2O_3$ glasses with high heavy metal oxide contents towards gamma irradiation revealed by collective optical, FTIR and ESR measurements. J Non-Cryst Solids. 2021;572:121090.

[12] Kaur K, Singh KJ, Anand V. Correlation of gamma ray shielding and structural properties of $PbO–BaO–P_2O_5$ glass system. Nucl Eng Des. 2015;285:31–8.

[13] Al-Harbi N, Al-Hadeethi Y, Bakry AS. Mechanical and radiation shielding features of bioactive glasses: $SiO_2–Na_2O–CaO–P_2O_5–B_2O_3$ for utilization in dental applications. J Non-Cryst Solids. 2021;552:120489.

[14] Kaewjaeng S, Boonpa W, Khrongchaiyaphum F, Kothan S, Kim HJ, Intachai N, et al. Influence of trivalent praseodymium ion on $SiO_2–B_2O_3–Al_2O_3–BaO–CaO–Sb_2O_3–Na_2O–Pr_2O_3$ glasses for X-Rays shielding and luminescence materials. Radiat Phys Chem. 2021;184:109467.

[15] Kaewjaeng S, Kothan S, Chaiphaksa W, Chanthima N, Rajaramakrishna R, Kim HJ, et al. High transparency $La_2O_3–CaO–B_2O_3–SiO_2$ glass for diagnosis x-rays shielding material application. Radiat Phys Chem. 2019;160:41–7.

[16] Tekin HO, Kavaz E, Altunsoy EE, Kamislioglu M, Kilicoglu O, Agar O, et al. Characterization of a broad range gamma-ray and neutron shielding properties of $MgO–Al_2O_3–SiO_2–B_2O_3$ and $Na_2O–Al_2O_3–SiO_2$ glass systems. J Non-Cryst Solids. 2019;518:92–102.

[17] Kaur P, Singh KJ, Thakur S, Singh P, Bajwa BS. Investigation of bismuth borate glass system modified with barium for structural and gamma-ray shielding properties. Spectrochim Acta A Mol Biomol Spectrosc. 2019 Jan;206:367–77.

[18] Shelby J. Introduction to glass science and technology. Royal Society of Chemistry; 2020.

[19] Osman AM, El-Sarraf MA, Abdel-Monem AM, El-Sayed, Abdo A. Studying the shielding properties of lead glass composites using neutrons and gamma rays. Ann Nucl Energy. 2015;78:146–51.

[20] Tekin HO, Kassab LR, Issa SA, Martins MM, Bontempo L, da Silva Mattos GR. Newly developed BGO glasses: synthesis, optical and nuclear radiation shielding properties. Ceram Int. 2020;46(8):11861–73.

[21] Nanda K, Kundu RS, Punia R, Mohan D, Kishore N. Resonant and non-resonant nonlinear optical properties of Er^{3+} modified $BaO–ZnO–B_2O_3$ glasses at 532 and 1550 nm. J Non-Cryst Solids. 2020;541:120155.

[22] Nanda K, Kundu RS, Sharma S, Mohan D, Punia R, Kishore N. Study of vibrational spectroscopy, linear and non-linear optical properties of Sm^{3+} ions doped $BaO–ZnO–B_2O_3$ glasses. Solid State Sci. 2015;45:15–22.

[23] Şakar E, Özpolat ÖF, Alım B, Sayyed MI, Kurudirek M. Phy-X/PSD: development of a user friendly online software for calculation of parameters relevant to radiation shielding and dosimetry. Radiat Phys Chem. 2020;166:108496.

[24] Mann KS, Mann SS. Py-MLBUF: development of an online-platform for gamma-ray shielding calculations and investigations. Ann Nucl Energy. 2021;150:107845.

[25] Nogami M, Nagakura T, Hayakawa T. Site-dependent fluorescence and hole-burning spectra of Eu^{3+}-doped $Al_2O_3–SiO_2$ glasses. J Lumin. 2000;86(2):117–23.

[26] Parchur AK, Prasad AI, Rai SB, Tewari R, Sahu RK, Okram GS, et al. Observation of intermediate bands in Eu^{3+} doped YPO4 host: Li^{+} ion effect and blue to pink light emitter. AIP Adv. 2012;2(3):032119.
[27] Mazurak Z, Bodył S, Lisiecki R, Gabryś-Pisarska J, Czaja M. Optical properties of Pr^{3+}, Sm^{3+} and Er^{3+} doped P_2O_5–CaO–SrO–BaO phosphate glass. Opt Mater. 2010;32(4):547–53.
[28] Bashter II, Makarious AS, Abdo ES. Investigation of hematite–serpentine and ilmenite-limonite concretes for reactor radiation shielding. Ann Nucl Energy. 1996;23(1):65–71.
[29] Mostafa AM, Issa SA, Zakaly HM, Zaid MH, Tekin HO, Matori KA, et al. The influence of heavy elements on the ionizing radiation shielding efficiency and elastic properties of some tellurite glasses: theoretical investigation. Results Phys. 2020;19:103496.
[30] Waly ES, Fusco MA, Bourham MA. Gamma-ray mass attenuation coefficient and half value layer factor of some oxide glass shielding materials. Ann Nucl Energy. 2016;96:26–30.
[31] El-Taher A, Zakaly HM, Pyshkina M, Allam EA, El-Sharkawy RM, Mahmoud ME, et al. A comparative study between fluka and microshield modeling calculations to study the radiation-shielding of nanoparticles and plastic waste composites. Z Anorg Allg Chem. 2021;647(10):1083–90.
[32] Tekin HO, Issa SA, Kilic G, Zakaly HM, Tarhan N, Sidek HA, et al. A systematical characterization of teo_2–v_2o_5 glass system using boron (iii) oxide and neodymium (iii) oxide substitution: resistance behaviors against ionizing radiation. Appl Sci (Basel). 2021;11(7):3035.
[33] Singh G, Gupta MK, Dhaliwal AS, Kahlon KS. Measurement of attenuation coefficient, effective atomic number and electron density of oxides of lanthanides by using simplified ATM-method. J Alloy Compd. 2015;619:356–60.
[34] Issa SA. Effective atomic number and mass attenuation coefficient of PbO–BaO–B_2O_3 glass system. Radiat Phys Chem. 2016;120:33–7.
[35] Elazaka AI, Zakaly HM, Issa SA, Rashad M, Tekin HO, Saudi HA, et al. New approach to removal of hazardous Bypass Cement Dust (BCD) from the environment: 20Na_2O-20$BaCl_2$-(60-x) B_2O_3-(x)BCD glass system and optical, mechanical, structural and nuclear radiation shielding competences. J Hazard Mater. 2021 Feb;403:123738.
[36] Ekinci N, Kavaz E, Özdemir Y. A study of the energy absorption and exposure buildup factors of some anti-inflammatory drugs. Appl Radiat Isot. 2014 Aug;90:265–73.
[37] Gerward L, Guilbert N, Bjorn Jensen K, Levring H. X-ray absorption in matter. Reengineering XCOM. Radiat Phys Chem. 2001;60(1-2):23–4.
[38] Gerward L, Guilbert N, Jensen KB, Levring H. WinXCom – a program for calculating X-ray attenuation coefficients. Radiat Phys Chem. 2004;71(3-4):653–4.
[39] Tekin HO, Kavaz E, Altunsoy EE, Kilicoglu O, Agar O, Erguzel TT, et al. An extensive investigation on gamma-ray and neutron attenuation parameters of cobalt oxide and nickel oxide substituted bioactive glasses. Ceram Int. 2019;45(8):9934–49.
[40] Saddeek YB, Issa SA, Alharbi T, Elsaman R, Abd Elfadeel G, Mostafa AM, et al. Synthesis and characterization of lead borate glasses comprising cement kiln dust and Bi_2O_3 for radiation shielding protection. Mater Chem Phys. 2020;242:122510.
[41] Rashad M, Hanafy TA, Issa SA. Structural, electrical and radiation shielding properties of polyvinyl alcohol doped with different nanoparticles. J Mater Sci Mater Electron. 2020;31(18):15192–7.
[42] Abou Elfadl A, Ismail AM, Mohammed MI. Dielectric study and AC conduction mechanism of gamma irradiated nano-composite of polyvinyl alcohol matrix with Cd0.9Mn0.1S. J Mater Sci Mater Electron. 2020;31(11):8297–307.
[43] Florian P, Sadiki N, Massiot D, Coutures JP. 27Al NMR study of the structure of lanthanum- and yttrium-based aluminosilicate glasses and melts. J Phys Chem B. 2007 Aug;111(33):9747–57.
[44] Ghosh S, Ghosh H. Sensitivity of As K-edge absorption to rare earth (RE) doping in Ca1–xRExFeAs2: a first principles study. J Phys Chem Solids. 2021;153:109993.
[45] Aktas B, Yalcin S, Dogru K, Uzunoglu Z, Yilmaz D. Structural and radiation shielding properties of chromium oxide doped borosilicate glass. Radiat Phys Chem. 2019;156:144–9.
[46] Yalcin S, Aktas B, Yilmaz D. Radiation shielding properties of Cerium oxide and Erbium oxide doped obsidian glass. Radiat Phys Chem. 2019;160:83–8.
[47] Mhareb MH, Alajerami YS, Sayyed MI, Dwaikat N, Alqahtani M, Alshahri F, et al. Radiation shielding, structural, physical, and optical properties for a series of borosilicate glass. J Non-Cryst Solids. 2020;550:120360.
[48] Al-Yousef HA, Sayyed MI, Alotiby M, Kumar A, Alghamdi YS, Alotaibi BM, et al. Evaluation of optical, and radiation shielding features of New phosphate-based glass system. Opt (Stuttg). 2021;242:167220.
[49] Almuqrin AH, Kumar A, Jecong JF, Al-Harbi N, Hannachi E, Sayyed MI. Li_2O–K_2O–B_2O_3–PbO glass system: optical and gamma-ray shielding investigations. Opt (Stuttg). 2021;247:167792.
[50] Mhareb MH, Alqahtani M, Alajerami YS, Alshahri F, Sayyed MI, Mahmoud KA, et al. Ionizing radiation shielding features for titanium borosilicate glass modified with different concentrations of barium oxide. Mater Chem Phys. 2021;272:125047.
[51] Singh S, Kaur R, Rani S, Sidhu BS. Physical, structural and nuclear radiation shielding behaviour of xBaO-(0.30-x)MgO-0.10Na_2O-0.10Al_2O_3-0.50B_2O_3 glass matrix. Mater Chem Phys. 2022;276:125415.
[52] Bashter II. Calculation of radiation attenuation coefficients for shielding concretes. Ann Nucl Energy. 1997;24(17):1389–401. Akkurt I, Malidarre RB. Gamma photon-neutron attenuation parameters of marble concrete by MCNPX code. Radiat Eff Defects Solids. 2021;176(9–10):906–18.
[53] Iskender A, Tekin HO. Radiological parameters for bismuth oxide glasses using phy-X/PSD software. Emerg Mater Res. 2020;9(3):1020–7. doi: 10.1680/jemmr.20.00209
[54] Rammah YS, Kumar A, Karem AAM, Raouf EM, El-Agawany FI, Susoy G, et al. SnO-reinforced silicate glasses and utilization in gamma-radiation-shielding applications. Emerg Mater Res. 2020;9(3):1000–8. doi: 10.1680/jemmr.20.00150
[55] Tekin HO, Issa SAM, Mahmoud KA, El-Agawany FI, Rammah YS, Susoy G, et al. Nuclear radiation shielding competences of Barium (Ba) reinforced borosilicate glasses. Emerg Mater Res. 2020;9(4):1131–44. doi: 10.1680/jemmr.20.00185
[56] Çelen YY. Gamma ray shielding parameters of some phantom fabrication materials for medical dosimetry. Emerg Mater Res. 2021;10(3):307–13.

[57] Çelen YY, Evcin A. Synthesis and characterizations of magnetite–borogypsum for radiation shielding. Emerg Mater Res. 2020;9(3):770–5. doi: 10.1680/jemmr.20.00098
[58] Lakshminarayana G, Kumar A, Tekin HO, Issa SA, Al-Buriahi MS, Dong MG, et al. Illustration of distinct nuclear radiation transmission factors combined with physical and elastic characteristics of barium boro-bismuthate glasses. Results Phys. 2021;105067:105067.
[59] Ilik E, Kavaz E, Kilic G, Issa SA, ALMisned G, Tekin HO. Synthesis and characterization of vanadium(V) oxide reinforced calcium-borate glasses: experimental assessments on Al_2O_3/BaO_2/ZnO contributions. J Non-Cryst Solids. 2022;580:121397.
[60] Lakshminarayana G, Kumar A, Tekin HO, Issa SAM, Al-Buriahi MS, Dong MG, et al. Probing of nuclear radiation attenuation and mechanical features for lithium bismuth borate glasses with improving Bi_2O_3 content for B_2O_3 + Li_2O amounts. Results Phys. 30 April 2021;25:104246. doi: 10.1016/j.rinp.2021.104246.
[61] ALMisned G, Elshami W, Issa S, Susoy G, Zakaly H, Algethami M, et al. Enhancement of gamma-ray shielding properties in cobalt-doped heavy metal borate glasses: the role of lanthanum oxide reinforcement. Mater (Basel). 2021;14(24):7703.
[62] Lakshminarayana G, Kumar A, Tekin HO, Issa SA, Al-Buriahi MS, Lee DE, et al. Binary B_2O_3-Bi_2O_3 glasses: scrutinization of directly and indirectly ionizing radiations s hielding abilities. J Mater Res Technol. 2020;9(6):14549–67.
[63] Ziegler JF, Ziegler MD, Biersack JP. SRIM – The stopping and range of ions in matter. Nucl Instrum Methods Phys Res Sect B. 2010;268:1818–23. doi: 10.1016/j.nimb.2010.02.091